Niche WNT5A regulates the actin cytoskeleton during regeneration of hematopoietic stem cells

Christina Schreck,[1]* Rouzanna Istvánffy,[1]* Christoph Ziegenhain,[3] Theresa Sippenauer,[1] Franziska Ruf,[1] Lynette Henkel,[2] Florian Gärtner,[4] Beate Vieth,[3] M. Carolina Florian,[5] Nicole Mende,[6] Anna Taubenberger,[7] Áine Prendergast,[8] Alina Wagner,[1] Charlotta Pagel,[1] Sandra Grziwok,[1] Katharina S. Götze,[1,9] Jochen Guck,[7] Douglas C. Dean,[10] Steffen Massberg,[4] Marieke Essers,[8] Claudia Waskow,[6] Hartmut Geiger,[5] Mathias Schiemann,[2] Christian Peschel,[1,9] Wolfgang Enard,[3] and Robert A.J. Oostendorp[1]

[1]Third Department of Internal Medicine, Klinikum rechts der Isar and [2]Department of Medical Microbiology, Immunology, and Hygiene, Technische Universität München, 81675 Munich, Germany
[3]Anthropology and Human Genomics, Department of Biology II and [4]Department of Internal Medicine I, Ludwig-Maximilian-Universität, 81377 Munich, Germany
[5]Institute of Molecular Medicine, University of Ulm, 89081 Ulm, Germany
[6]Regeneration in Hematopoiesis and Animal Models in Hematopoiesis, Institute for Immunology, TU Dresden, 01309 Dresden, Germany
[7]Biotechnology Center TU Dresden, 01307 Dresden, Germany
[8]German Cancer Research Center (DKFZ) and Heidelberg Institute for Stem Cell Technology and Experimental Medicine, 69120 Heidelberg, Germany
[9]German Cancer Consortium, DKFZ, 69120 Heidelberg, Germany
[10]Molecular Targets Program, James Brown Cancer Center, University of Louisville Health Sciences Center, Louisville, KY 40202

Here, we show that the *Wnt5a*–haploinsufficient niche regenerates dysfunctional HSCs, which do not successfully engraft in secondary recipients. RNA sequencing of the regenerated donor Lin⁻ SCA-1⁺ KIT⁺ (LSK) cells shows dysregulated expression of ZEB1-associated genes involved in the small GTPase-dependent actin polymerization pathway. Misexpression of DOCK2, WAVE2, and activation of CDC42 results in apolar F-actin localization, leading to defects in adhesion, migration and homing of HSCs regenerated in a *Wnt5a*–haploinsufficient microenvironment. Moreover, these cells show increased differentiation in vitro, with rapid loss of HSC-enriched LSK cells. Our study further shows that the *Wnt5a*–haploinsufficient environment similarly affects BCR–ABL^p185 leukemia–initiating cells, which fail to generate leukemia in 42% of the studied recipients, or to transfer leukemia to secondary hosts. Thus, we show that WNT5A in the bone marrow niche is required to regenerate HSCs and leukemic cells with functional ability to rearrange the actin cytoskeleton and engraft successfully.

INTRODUCTION

Hematopoietic stem cells (HSCs) are defined by their ability to repopulate the blood cell system in steady-state and transplantation settings. The interplay of intrinsic (donor-derived) and extrinsic (host-derived) factors in successful engraftment is not entirely understood. Several intrinsic subprocesses enable HSCs to engraft: the ability of HSCs to find their niche, migrate into it, lodge there, proliferate, self-renew, and differentiate into mature hematopoietic cells without exhaustion or leukemic transformation. The extrinsic factors are orchestrated by these cellular events and attract HSCs, as well as secreted factors, to the niche, restrict unbridled HSC activation (Renström et al., 2009; Istvanffy et al., 2011; Ruf et al., 2016),

prevent HSC senescence, promote survival, and guide proliferation and differentiation.

Interference with any of the engraftment subprocesses delays regeneration of the hematopoietic system and reestablishment of the pool of quiescent HSCs. Wnt signaling maintains the balance between HSC quiescence and HSC activation, through coupling of Frizzled receptors to G-proteins and Disheveled to the β- and γ-catenin–dependent canonical, as well as calcium-dependent or small GTPase-dependent, noncanonical pathways (Dijksterhuis et al., 2014). Catenin-dependent Wnt signaling is required for differentiation and HSC self-renewal through precise regulation of its amplitude: low levels of catenin activation promotes self-renewal, whereas higher levels drive differentiation (Luis et al., 2011). The further downstream mechanisms are likely to involve different degrees of oxidative stress and the ability to resolve DNA double-strand breaks (Lento et al., 2014). In leuke-

Supplemental material can be found at:
http://doi.org/10.1084/jem.20151414

mia models, activated β-catenin is required for survival and proliferation in MLL-AF9– (Wang et al., 2010) and BCR-ABL–driven leukemia (Zhao et al., 2007). Although it is not clear how catenin is up-regulated in leukemia, progression of BCR-ABL–driven leukemia is accelerated by activation of catenin, which may, at least in part, be caused by mis-splicing of GSK3β (Abrahamsson et al., 2009).

WNT5A is both glycosylated and palmitoylated, and is the main stimulator of noncanonical Wnt signaling. WNT5A is induced in inflammatory niche responses (Rauner et al., 2012), but its role for normal and malignant hematopoiesis is poorly understood. The expression of $Wnt5a$ is strong in stromal cells, but is also found in B220$^+$ lymphocytes (Liang et al., 2003). We previously found that $Wnt5a$ is particularly strongly expressed in stromal cells, which maintain HSCs under noncontact conditions (Buckley et al., 2011). In addition, WNT5A promotes HSC maintenance in the absence of stromal cells through inhibition of canonical signaling (Murdoch et al., 2003; Nemeth et al., 2007). These reports are apparently conflicting with our finding that WNT5A expression is up-regulated during aging in HSCs and, as such, impaired HSC regenerative capacity through CDC42-mediated inhibition of actin polarization (Florian et al., 2013).

To shed more light on how WNT5A produced by the microenvironment regulates HSCs, we studied the role of Wnt5a in the regenerative response of normal hematopoiesis and in BCR-ABL–driven leukemogenesis. Because $Wnt5a^{-/-}$ mice die just before birth as a result of multiple tissue developmental defects, we used adult $Wnt5a$-haploinsufficient mice (Yamaguchi et al., 1999). We find that HSCs regenerated in a $Wnt5a^{+/-}$ environment, show severe defects in HSC engraftment. Gene expression analysis coupled to functional assays show that the HSCs regenerated in the $Wnt5a$-haploinsufficient niche display up-regulated small GTPase-mediated noncanonical signaling-impaired F-actin polarization. These alterations results in decreased adhesion, migration, and homing. In addition, we observed similar effects in BCR-ABL^{p185} expressing cells that failed to develop leukemia in secondary recipients. These results indicate that the $Wnt5a$-haploinsufficient niche may prevent engraftment of leukemia-initiating cells.

RESULTS
Characterization of phenotype and HSC function of $Wnt5a^{+/-}$ mice
To study the role of Wnt5a in HSC regeneration, we used heterozygous Wnt5a knockout ($Wnt5a^{+/-}$) mice, because homozygous knockout mice die just before birth (Yamaguchi et al., 1999; Liang et al., 2003). $Wnt5a^{+/-}$ mice are viable and fertile, and adult $Wnt5a^{+/-}$ mice show a 1.7-fold increase in Lin$^-$IL-7R$^+$ common lymphoid progenitors (CLPs), unchanged myeloid progenitors (MPs), and an unchanged clonogenic activity of progenitors (Fig. 1, A and B; and Fig. S1 A). Furthermore, we observed a 1.4-fold decrease in the Lin$^-$ SCA-1$^+$ KIT$^+$ (LSK) population, which is mainly a result of a 1.7-fold de-

crease in CD34$^+$ LSKs, because the CD34$^-$ CD150$^+$ LSKs are unchanged (Fig. 1 A).

To determine whether the reduction in LSKs reflects a reduced HSC pool, we sorted HSC-enriched CD34$^-$ CD150$^+$ LSKs from the $Wnt5a^{+/+}$ (WT) and $Wnt5a^{+/-}$ mice and transplanted these in equal numbers into congenic WT recipients (Fig. 1 C). We found that, despite the known expression of $Wnt5a$ in CD34$^-$ Flk2$^-$ LSK cells (Florian et al., 2013) and B lymphocytes (Liang et al., 2003), lymphoid and myeloid engraftment of $Wnt5a^{+/-}$ LT-LSKs was similar in primary, secondary, and tertiary recipients (Fig. 1, D–H; and Fig. S1, B and C). Also, engraftment of WT and $Wnt5a^{+/-}$ LT-LSKs in the BM (Fig. 1, I–K) was unchanged. Additionally, amplification of the donor pool of WT and $Wnt5a^{+/-}$ LT-LSKs after each round of transplantations was not significantly different (Fig. 1, L and M).

The $Wnt5a^{+/-}$ niche regenerates HSCs with defective regenerative ability
To test the effect of extrinsic niche WNT5A on HSCs regeneration, we transplanted WT HSCs into WT and $Wnt5a^{+/-}$ recipient mice (Fig. 2 A). In primary recipients, WT HSCs regenerated similarly in peripheral blood (PB), SPLs, and BM with comparable percentage of lymphoid and myeloid populations in PB (Fig. 2, B and C). Moreover, the absolute numbers of engrafted Lin$^-$, MP, LSKs and CD34$^-$ CD150$^+$ LSKs was similar 16 wk after transplantation (Fig. 2, D and E). To test the self-renewing activity of HSCs engrafted in WT (LSK-WT) and $Wnt5a^{+/-}$ (LSK-5a) recipients, we serially transplanted equal numbers of donor LSKs. Surprisingly, in three independent experiments, we did not detect engraftment of >1% lymphoid or myeloid donor cells in the PB of secondary recipients at 5, 10, and 16 wk after transplantation from LSK-5a cells (Fig. 2, F–H). In addition, the LSK compartment was not regenerated by LSK-5a cells (Fig. 2, I and J). Transplanting higher numbers of LSK-5a cells showed an estimated 17-fold lower frequency of repopulating HSCs (Fig. 2 G). Hence, we find that regeneration of the HSC compartment in the $Wnt5a$-haploinsufficient environment is severely compromised.

To find out whether aberrant HSC regeneration is caused by altered niche composition, we first confirmed decreased WNT5A content in the cultured endosteal cells of $Wnt5a^{+/-}$ mice compared with their WT littermates (Fig. 3 A). We identified that WNT5A expression in freshly isolated collagenase-treated BM cells was restricted to multipotent stromal cells (MSCs; Fig. 3 B). Additionally, we did not observe any gross abnormalities in the niche architecture as detected by laminin- (endothelial cells; ECs) and SCA-1–stained (ECs and MSCs) bone sections (Fig. 3 C).

In the transplanted primary recipients, the number of ECs, osteoblastic cells (OBCs), and MSCs was identical in WT and $Wnt5a^{+/-}$ recipient mice (Fig. 3, D–F). To find out whether these cells from WT and $Wnt5a^{+/-}$ mice show differences in gene expression, we generated RNA-Seq libraries
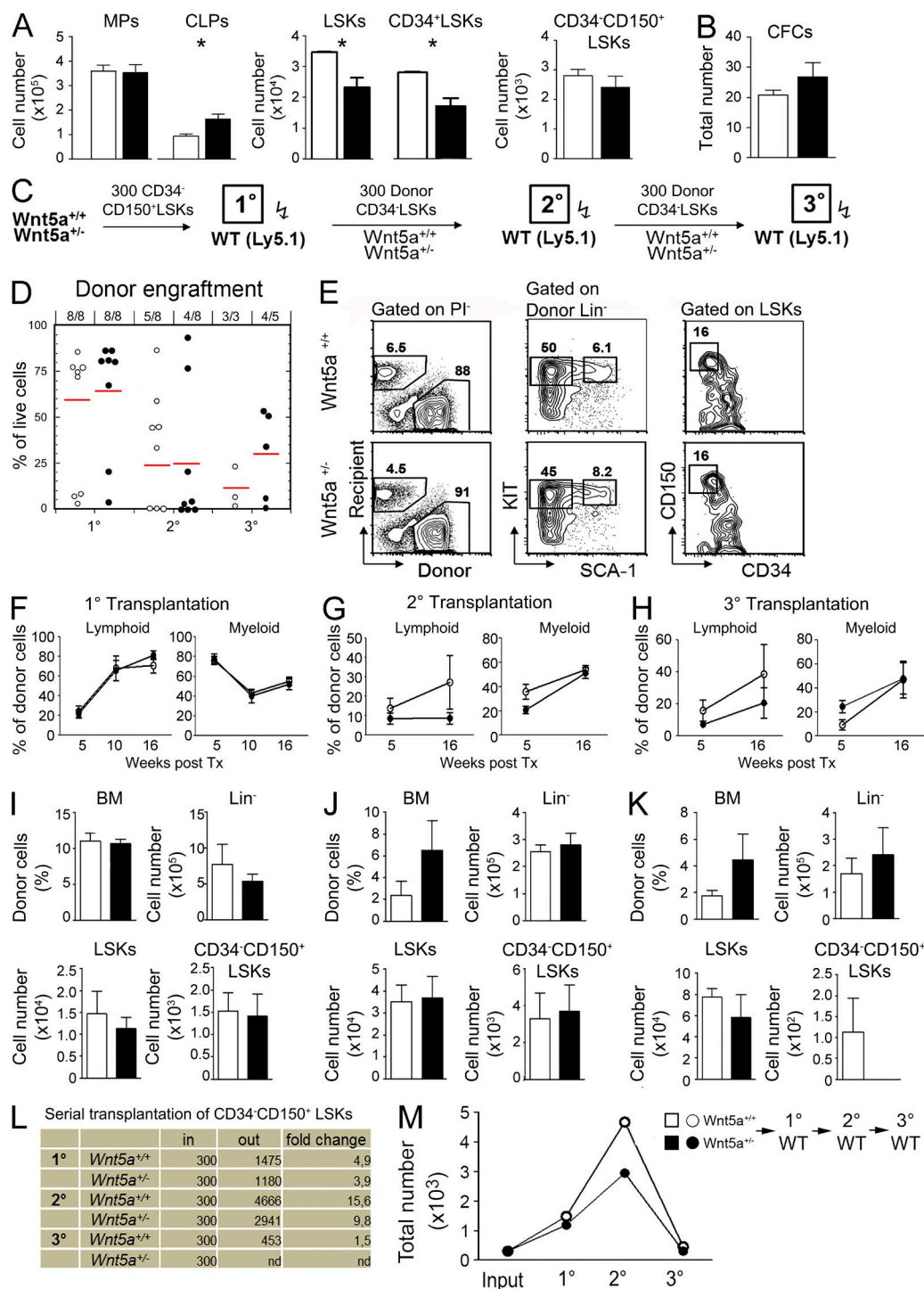
Figure 1. LT–HSCs from *Wnt5a*^+/− mice show unchanged repopulating capacity. (A) Absolute numbers of MPs, CLPs, CD34^+ LSKs, and CD34^− CD150^+ LSKs in the BM of *WT* and *Wnt5a*^+/− mice (*n* = 15 each). (B) Total numbers of CFCs. (C) Experimental design. Serial transplantations of HSCs of both genotypes. (D) Donor engraftment in the BM of primary, secondary, and tertiary (1°, 2°, and 3°) recipient mice. The number of engrafted mice compared to the total number of transplanted mice is also shown. (E) Representative FACS plots of the BM from the 1° recipients (*n* = 8). (F–H) The lymphoid and myeloid engraftment in the PB of 1°, 2°, and 3° recipients 5, 10, and 16 wk after Tx, respectively. (I–K) The corresponding percentage of donor cells and absolute numbers of HSCs and progenitors in the BM 16 wk after transplantation. (L) The total number of transplanted and repopulated LT-LSKs in serial transplantations (*n* = 8) in 1° and 2° recipients. *n* = 4 (WT); n = 5 (*Wnt5a*^+/−), respectively, in the 3° recipients. (M) Numbers of donor CD34^− CD150^+ LSKs regenerated in 1°, 2°, and 3° recipients. Shown are the results of two independent experiments. Column plots show the mean ± SEM. *, P < 0.05 (Student's *t* test).
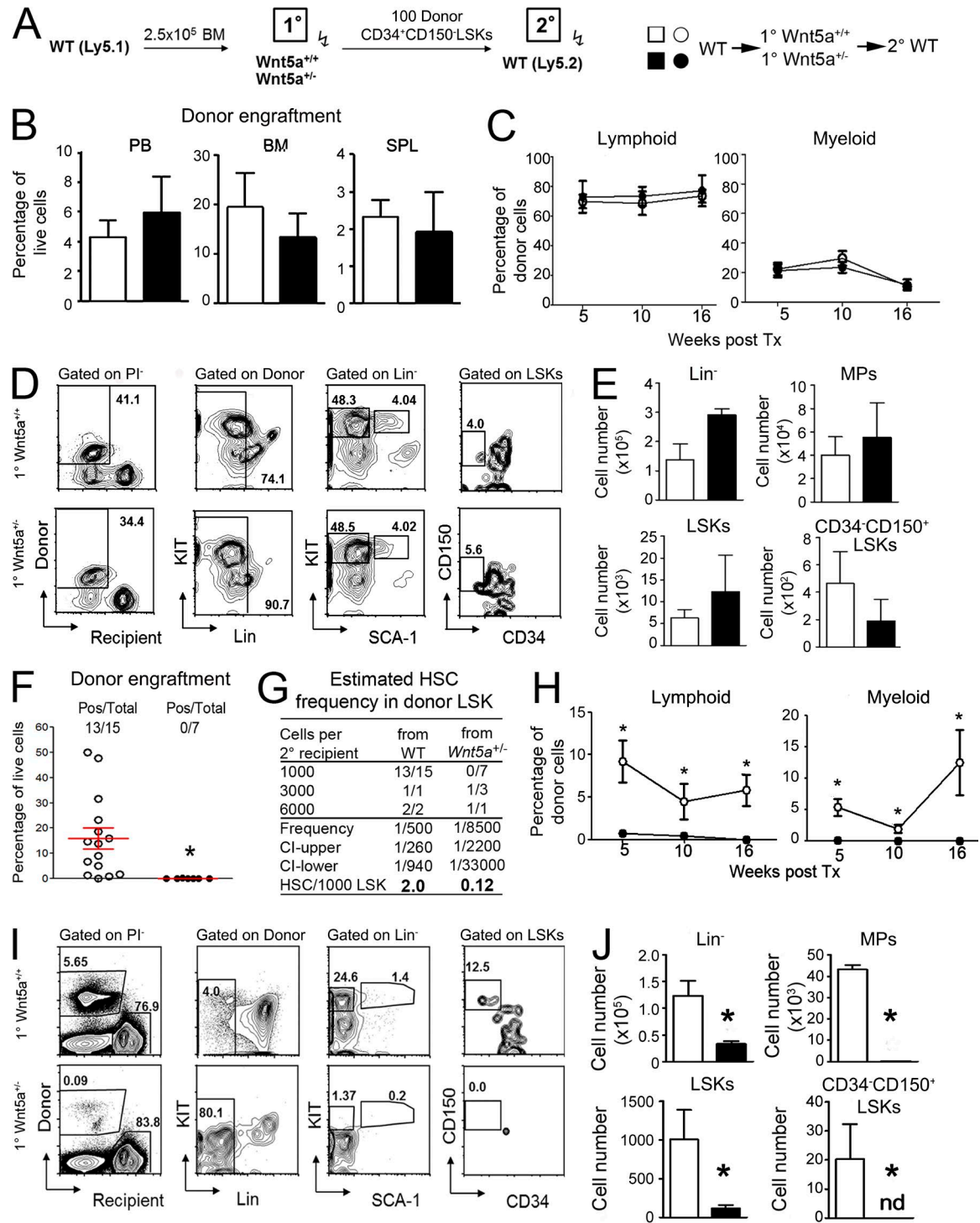
Figure 2. **Impaired engraftment of WT LSKs after exposure to *Wnt5a*–deficient environment (LSK–5a) compared with regeneration in WT recipients (LSK–WT).** (A) Experimental design. Serial transplantations of WT cells into recipients of both genotypes. (B) The donor engraftment in PB, BM, and spleens of recipients (WT, n = 10; *Wnt5a*^{+/−}, n = 14). (C) Lymphoid and myeloid engraftment in the PB of 1° recipients 5, 10, and 16 wk after transplantation. (D) Representative FACS plots of BM from 1° recipients. (E) Absolute numbers of engrafted Lin⁻, MPs, LSKs, and CD34⁻ CD150⁺ LSKs in the BM of 1° recipients. (WT, *n* =15; *Wnt5a*^{+/−}, *n* = 7). Presented are the results of three independent experiments. (F) The donor engraftment in BM of 2° recipients. The engraftment with >1% of lymphoid and myeloid cells was defined as positive. (G) Limiting dilution analysis of 1,000, 3,000, and 6,000 1° LSKs in the PB of the recipient mice. (H) Lymphoid and myeloid engraftment in PB of 2° mice after 5, 10, and

from 3 independent pools of sorted MSCs (2.5–4×10^3 cells) and OBCs (2–3×10^3 cells) from recipient mice 16 wk after transplantation (Fig. 3 G). Samples were grouped according to the cell identity and genotype in the principal component analysis (PCA; Fig. 3 G). Unsurprisingly, comparison of MSCs and OBCs show a large amount of differentially expressed genes (DEGs; Fig. 3 H). Comparisons of reported niche and pericyte genes in *WT* and *Wnt5a*$^{+/-}$ MSCs and OBCs were very similar, other than decreased *Spp1* in OBCs (Fig. 3, I–K; and Table S3). We found only 79 significantly DEGs between MSCs from WT and *Wnt5a*$^{+/-}$ recipients (Fig. 3 L). The analysis of specific pathways or biological processes was not informative (Table S4).

Gene expression of LSK cells regenerated in *WT* and *Wnt5a*$^{+/-}$ mice diverges

To determine how regenerated LSKs respond to the two environments, we generated RNA-Seq libraries from sorted 1,500 to 3,000 LSK-WT and LSK-5a (Fig. 4 A) and mapped in a mean of 12.3 million sequence reads per library. The mapped samples were grouped according to the recipient genotype in the principle component analysis (Fig. 4 B). From the 14,029 genes tested, 656 were differently expressed between LSK-5a and LSK-WT cells (FDR < 0.05; Fig. 4 C and Table S5). These DEGs were enriched in the pathways with protein processing, inositol phosphate metabolism, and cell cycle and actin cytoskeleton regulation among the 10 most enriched pathways (Fig. 4 D and Table S6). Surprisingly, no enrichment for DEGs annotated in the Wnt signaling pathway (Kyoto Encyclopedia of Genes and Genomes [KEGG] ID, mmu04310) or other ontology categories related to the Wnt signaling was found (unpublished data). Indeed, using manual curation, we found that LSK-WT and LSK-5a cells express similar levels of Fzd receptors, as well as mediators of canonical or calcium-dependent noncanonical pathways (Table S5). Interestingly, regulation of actin cytoskeleton (KEGG ID mmu04810) is the pathway with the most genes up-regulated in LSK-5a cells (Fig. 4, D and E). We confirmed these results on the protein level (Fig. 4 F). Interestingly, alterations in protein levels of DOCK2, CDC42, WAVE2, and F-Actin was correlated with a decrease in polarized localization (Fig. 4 G).

A closer look at donor HSC-enriched subpopulations showed that F-actin is also distributed in an apolar manner in CD34$^-$ LSK-5a cells (Fig. 4 H). Furthermore, in accordance with our finding that expression of canonical Wnt-related mediators is not altered in LSK-5a cells, we also found no differences in protein levels of the main mediators β-catenin and MYC (Fig. 4 I). These results are reminiscent of our previous finding in aged HSCs, which show reduced F-actin po-

larization caused by CDC42 activation (Florian et al., 2013). Indeed, a pull-down assay showed that the relative quantity of GTP-binding activated CDC42 is higher in sorted donor Lin$^-$ cells from primary *Wnt5a*$^{+/-}$ recipients (Fig. 4 J).

To interrogate which transcription factors may contribute to the differential gene expression in LSK-5a cells, the Integrated System for Motif Activity Response Analysis (ISMARA) prediction tool showed enrichment of DEGs in ZEB1, AIRE, FOXQ1, NKX2-2,8, and NFATC1.3 motifs (Fig. 4 K). Importantly, genes in the actin regulatory pathway are enriched in ZEB1 motifs (Fig. 4 L). Indeed, in *Zeb1*-KO MEFs, *Arhgef7*, *Pak4*, and *Wasf2* were found to be directly regulated by ZEB1 (Fig. 4 M). Given these findings, we considered actin regulation as a promising mechanism that could explain why WT LSKs regenerated in the *Wnt5a*-haploinsufficient niche lose their stemness.

LSK cells regenerated in *Wnt5a*$^{+/-}$ mice show defective actin–dependent responses

The actin-driven cellular polarization is at the basis of migratory processes required for HSC engraftment. To interrogate these processes, we compared the general mechanical properties, adhesion, chemotaxis, and homing properties with LSK-WT and -5a cells (Fig. 5 A). We did not observe differences in the diameter and the cell stiffness of LSK-5a as detected with apparent Young's modulus (Fig. 5, B and C). CXCL12 promotes F-actin polarization (Voermans et al., 2001), but did not rescue the apolar distribution of F-actin in LSK-5a cells (Fig. 5, D and E).

To determine functional consequences of reduced actin assembly, in a first experiment, we found that sorted LSK-5a cells only poorly adhered to VCAM1-Ig–coated slides (Fig. 5 F). In a second experiment, we found that although the starting number and composition of Lineage-depleted donor cells from WT and *Wnt5a*$^{+/-}$ recipients was similar, migration of the LSK-5a cells and Lin$^-$ and MPs from *Wnt5a*$^{+/-}$ recipients toward CXCL12 was profoundly less efficient than their *WT* counterparts in a Boyden chamber assay (Fig. 5 G).

To find out whether in vivo responses of LSK-5a were affected in a manner similar to the in vitro adhesion and migration, we injected lineage-depleted donor cells recovered from WT and *Wnt5a*$^{+/-}$ recipients into irradiated WT recipient mice. In these experiments, we found strongly reduced homing of Lin$^-$ Kit$^+$, MP, and LSK donor subpopulations from *Wnt5a*$^{+/-}$ recipients 16 h after injection (Fig. 5, H and I). This confirmed the migratory defects of hematopoietic cells regenerated in *Wnt5a*$^{+/-}$ recipients in vivo.

To determine whether the remaining LSK-5a cells that do home to the marrow fail to engraft as a result of decreased cell division or reduced survival, we set up single-cell cultures

16 wk after transplantation. (I) Representative FACS plots of BM from 2° recipients 16 wk after transplantation. (J) The absolute numbers of donor Lin$^-$, MPs, LSKs, and LT-LSKs in BM of 2° mice. (WT, $n = 15$; *Wnt5a*$^{+/-}$, $n = 7$). These are the combined results of three independent experiments shown as mean $\pm$ SEM. *, P < 0.05 (Student's *t* test).
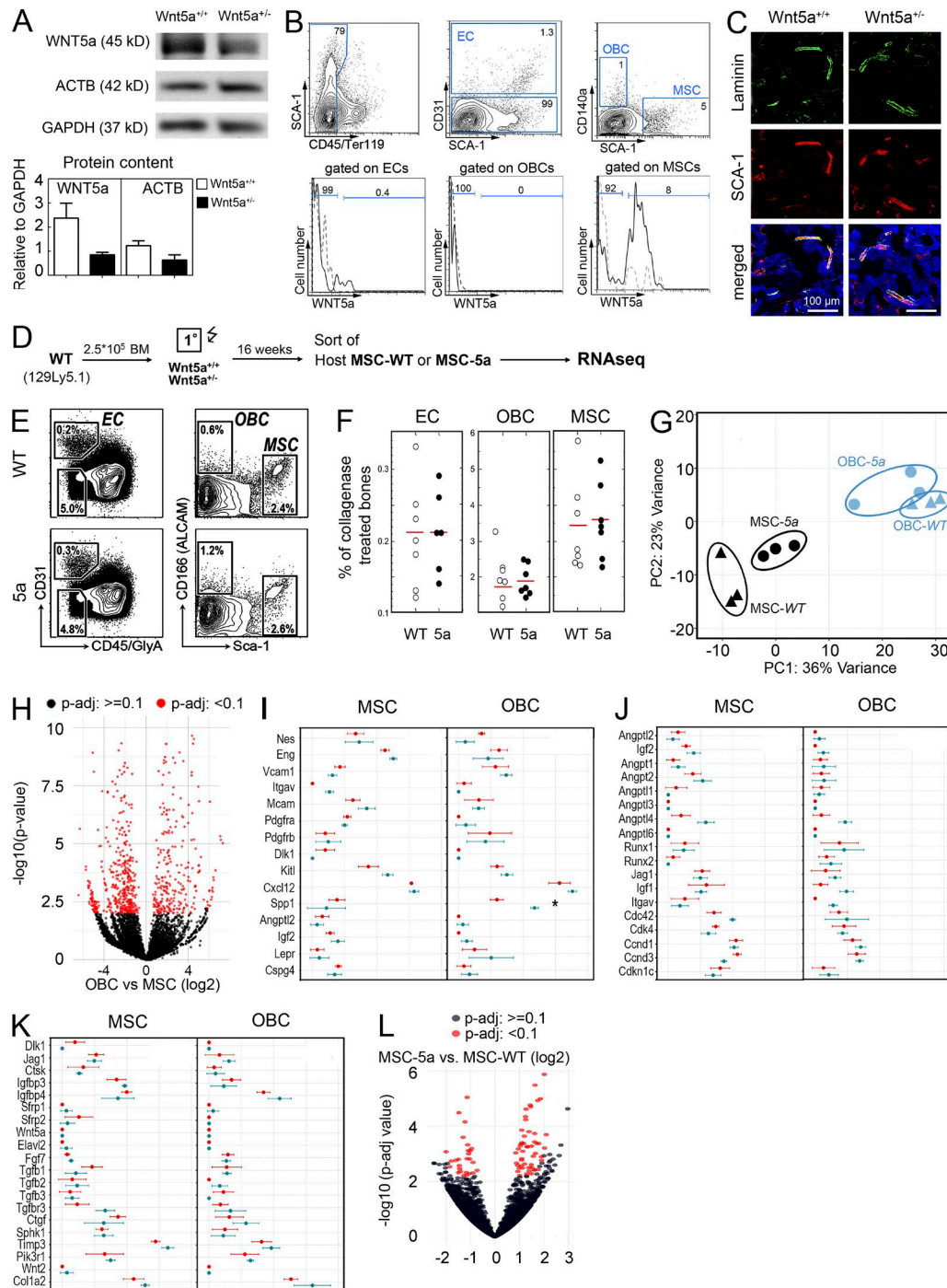
Figure 3. WNT5A expression and analysis of the niche cells after transplantation. (A) Western blots and protein content in cultured stromal cells from *WT* and *Wnt5a*^{+/−} mice quantified with ImageJ software and presented as relative values to GAPDH (*n* = 6). (B) Representative FACS plots of intracellular WNT5A expression in MSCs, OBCs, and ECs. (C) Laminin and SCA-1 expression in bone sections of mice from both genotypes (*n* = 3). (D) Experimental workflow. RNA-Seq on OBCs and MSCs isolated form the 1° recipients of both genotypes (*n* = 3). (E) Representative FACS gating for sorting of niche cells. (F) The percentages of ECs, OBCs, and MSCs in 1° recipients of both genotypes. (G) The two-dimensional representation of RNA-Seq probes by PCA computed using the 400 most variable gene expression values. (H) Volcano plot comparison of MSCs and OBCs irrespective of recipient genotype. (I–K) Expression of niche and perivascular genes compiled from published reports (Khan et al., 2016; I and J), and our own previous work (K). (L) Volcano plot of the differential gene expression in MSCs from *WT* and *Wnt5a*^{+/−} recipients. For each detected gene, differential gene expression testing is shown as $\log_2$ fold-change against $-\log_{10}$ (p-adj). Significantly (FDR < 0.1) DEGs are shown in red.
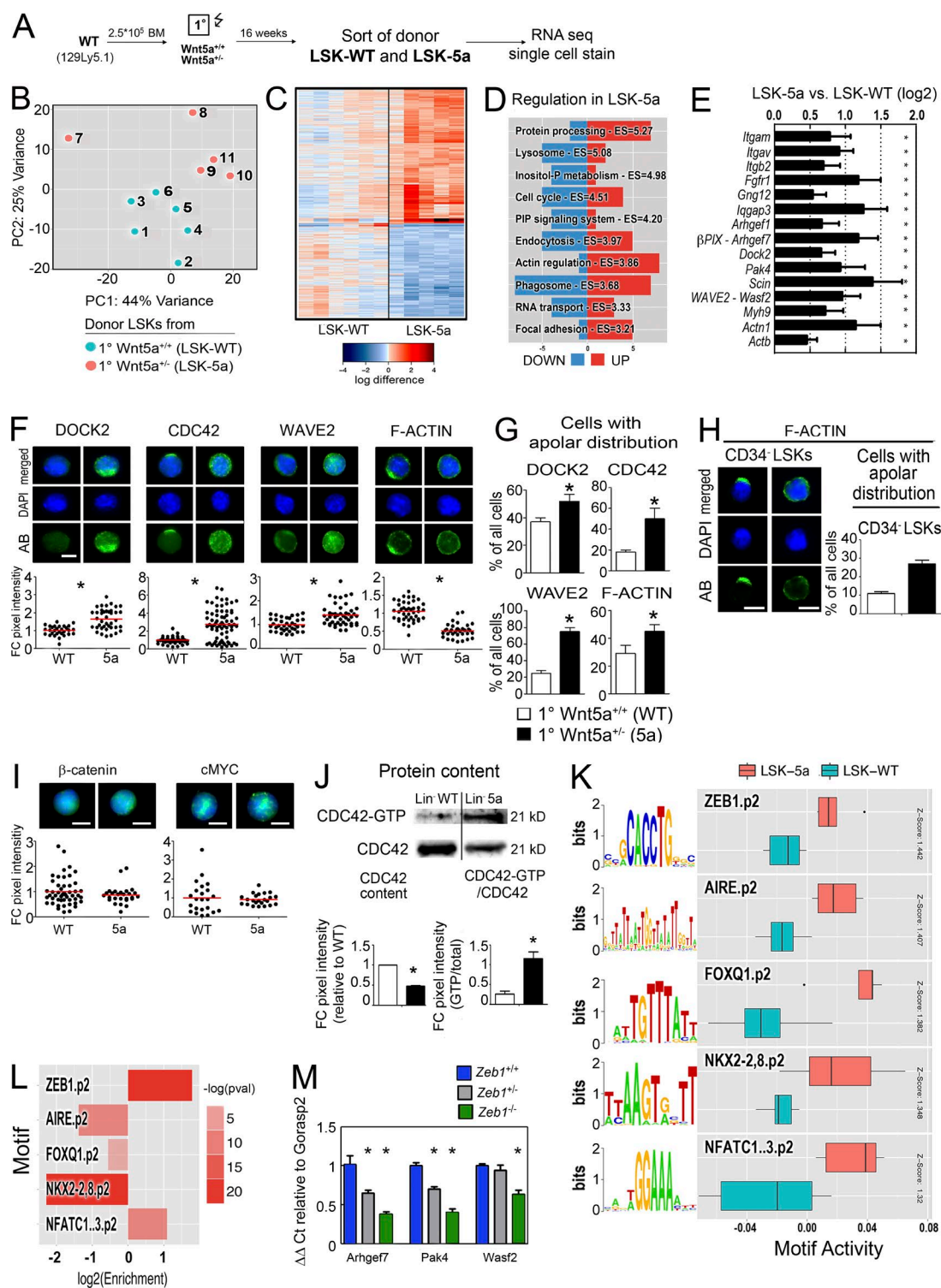
Figure 4. **The actin-regulatory pathway is dysregulated in LSK-5a cells.** (A) Experimental workflow. The RNA-seq analysis of donor LSKs from 1° recipients of both genotypes (WT, $n = 6$; Wnt5a$^{+/-}$, $n = 5$). (B) Plot showing the two-dimensional representation of RNA-Seq samples by PCA computed using the 500 most variable gene expression values. (C) Shown are expression values of significantly (FDR < 0.05) DEGs in LSK-WT and LSK-5a samples. Rows denote genes and columns denote samples of donor LSKs isolated from individual recipient mice. Values are normalized to the mean log-expression in LSK-WT samples. (D) The 10 KEGG pathways with the strongest significant (FDR < 0.05) enrichment of DEGs. Bars show the number of significantly up- (red) or down-regulated (blue) genes in the corresponding pathway and are sorted according to the enrichment score (ES). Pathways containing <5 DEGs

(Wohrer et al., 2014; Istvánffy et al., 2015). These showed that cell division and survival of CD34⁻ LSK-5a cells were similar to CD34⁻ LSK–WT cells (Fig. 5, J and K). This experiment further showed that addition of rWNT5a does not enhance or reduce the clone size or the number of CD34⁻ LSK-5a cells dividing (Fig. 5, J and K). Interestingly, however, addition of rWNT5A increases differentiation of CD34⁻ LSK-5a cells, with almost complete loss of LSKs, whereas their *WT* counterparts preserved LSK cells (Fig. 5, L and M).

To assess whether WNT5A-mediated cross talk between Wnt5a-competent WT HSCs and whether the *Wnt5a*$^{+/-}$ niche is responsible for the reduced engraftment in secondary transplants, we transplanted HSCs from *Wnt5a*$^{+/-}$ donors into WT (HET/WT) or *Wnt5a*$^{+/-}$ recipients (HET/HET; Fig. 6 A). This experiment showed that *Wnt5a*$^{+/-}$ donor LSKs regenerated in *Wnt5a*$^{+/-}$ recipients behaved essentially similar as LSK-5a cells in both primary and secondary transplants (Fig. 6, B and C), with a low detection of mostly myeloid engraftment in HET/HET mice 5 wk after secondary (2°) transplantation. Moreover, as in LSK-5a cells, the polar distribution of DOCK2, WAVE2, and F-actin was also decreased in *Wnt5a*$^{+/-}$ CD34⁻ LSK cells regenerated in *Wnt5a*$^{+/-}$ recipients (HET/HET; Fig. 6, D–F).

The *Wnt5a*$^{+/-}$ niche does not support the development of BCR-ABL–driven leukemia

To find out whether Wnt5a deficiency affects leukemogenesis, we studied a model of BCR-ABL^{p185}–induced leukemia (Kelliher et al., 1991). Neonatal *WT* mice transplanted with BM cells transduced with an e1a2 BCR-ABL^{p185} expression vector succumbed to lympho–myeloproliferative disease (LMPD) characterized by increasing cell numbers in the periphery and splenomegaly with a lag time of 58 d (Fig. 7, A–D). The juvenile LMPD mice mostly suffer from a mixed lymphoid-myeloid (42%), lymphoid (42%), and in remaining cases a myeloid leukemia (16%). In neonatal *Wnt5a*$^{+/-}$ recipients, we observed a significant number of mice (12/28, 43%) which did not develop leukemia. These disease-free recipients showed essentially similar numbers of GFP⁺ blood cells and spleen weights as the MSCV-IRES-GFP backbone control vector–transduced donor cells (Fig. 7 D). Sixteen *Wnt5a*$^{+/-}$ recipients transplanted with BCR-ABL^{p185+} cells developed a lethal LMPD with a high GFP⁺ cell engraftment, and higher

PB count and more pronounced splenomegaly than leukemic WT recipients (Fig. 7 D).

To assess leukemogenic potential of cells from the primary recipients, we transferred 1×10^6 GFP⁺ spleen cells into secondary WT recipients (Li et al., 1999). These secondary recipients from BCR-ABL^{p185} WT cells all caused secondary LMPD with a lag time of 38 d (Fig. 7 E). In contrast, only one of eleven secondary recipients of BCR-ABL^{p185+} cells from leukemic *Wnt5a*$^{+/-}$ recipients was able to transfer leukemia (Fig. 7 E) and failed to engraft a significant number of GFP⁺ cells (not depicted).

To determine whether BCR-ABL^{p185+} cells from *Wnt5a*$^{+/-}$ recipients show similar defects in actin regulation as LSK-5a cells, we isolated GFP⁺ from the BM of primary recipients with LMPD to study cellular signaling and their migratory properties. As we were unable to isolate sufficient GFP⁺ LSK cells from the BM for functional analyses (Fig. S3), we studied GFP⁺ B cells from the BM of LMPD mice instead. Immunofluorescent analysis showed increased expression of CDC42, WAVE2, and F-actin, as well as loss of CDC42, WAVE2, and F-actin polarization in BCR-ABL⁺ cells from *Wnt5a*$^{+/-}$ recipients (Fig. 7 F). Unlike normal LSK-5a cells, the polarized expression of DOCK2, was not affected (Fig. 7 G). In contrast to normal LSK-5a cells, and in accord with the more severe LMPD in *Wnt5a*$^{+/-}$ recipients (Fig. 7 D), in leukemic cells we find an increased expression of the canonical Wnt mediators DVL2 and β-catenin (Fig. 7 H).

To find out whether the changes in polarized localization of F-actin, CDC42, and WAVE2 have similar functional consequences as in LSK-5a cells, we set up experiments to study actin-dependent cellular responses on leukemic B cells. These experiments demonstrated that leukemic GFP⁺ cells show reduced CXCL12-stimulated F-actin polarization (Fig. 7 I), but that adhesion to VCAM-1 is only marginally reduced (Fig. 7 J). Yet, GFP⁺ BCR-ABL^{p185+} B cells show reduced chemotaxis toward CXCL12 (Fig. 7 K). Thus, our results show that similar to LSK-5a cells, leukemic BCR-ABL^{p185+} B cells formed in Wnt5a$^{+/-}$ recipients demonstrate defective actin regulation, and fail to transfer BCR-ABL^{p185+} LMPD.

DISCUSSION

One of the major goals in stem cell biology is to understand the factors involved in successful engraftment of stem cells

were discarded (Table S6). (E) Graph showing the comparison of the ratio of the mean expression of differentially up-regulated genes in the regulation of the actin cytoskeleton pathway between LSK-WT and LSK-5a. (F) The DOCK2, CDC42, WAVE2, and F-actin protein expression in LSK-WT and -5a counter stained with DAPI. The fluorescence intensities were quantified with ImageJ software. (G) The percentage of cells with apolar expression of respective proteins in 1° LSKs from *WT* or *Wnt5a*$^{+/-}$ recipients. (H) F-actin expression in CD34⁻ subfractions of 1° LSKs and the percentage of cells with apolar distribution of the F-actin complex. (I) The β–catenin and c-MYC expression in 1° LSKs of both genotype recipients. (J) The protein content of the active CDC42-GTP in donor Lin⁻ cells of 1° recipients relative to the total CDC42. The intensities on Western blot calculated with ImageJ software. (K) Transcription factor binding motifs with the highest influence on gene expression changes between LSK-WT (blue boxes) and LSK-5a (pink boxes). Shown are the changes in motif activities with corresponding z-scores of the averaged ISMARA analysis. (L) Enrichment analysis for the KEGG pathway actin regulation in genes with promoters containing transcription factor binding motifs identified by ISMARA. The log-transformed enrichment scores are plotted and shaded according to significance (Fisher's exact test). (M) The mRNA content of ZEB1 target genes in in *Zeb1* mutant and WT MEFs relative to the *Gorasp2*. *, P < 0.05 (E, G, J, and M, Student's *t* test; F and I, MWU test).
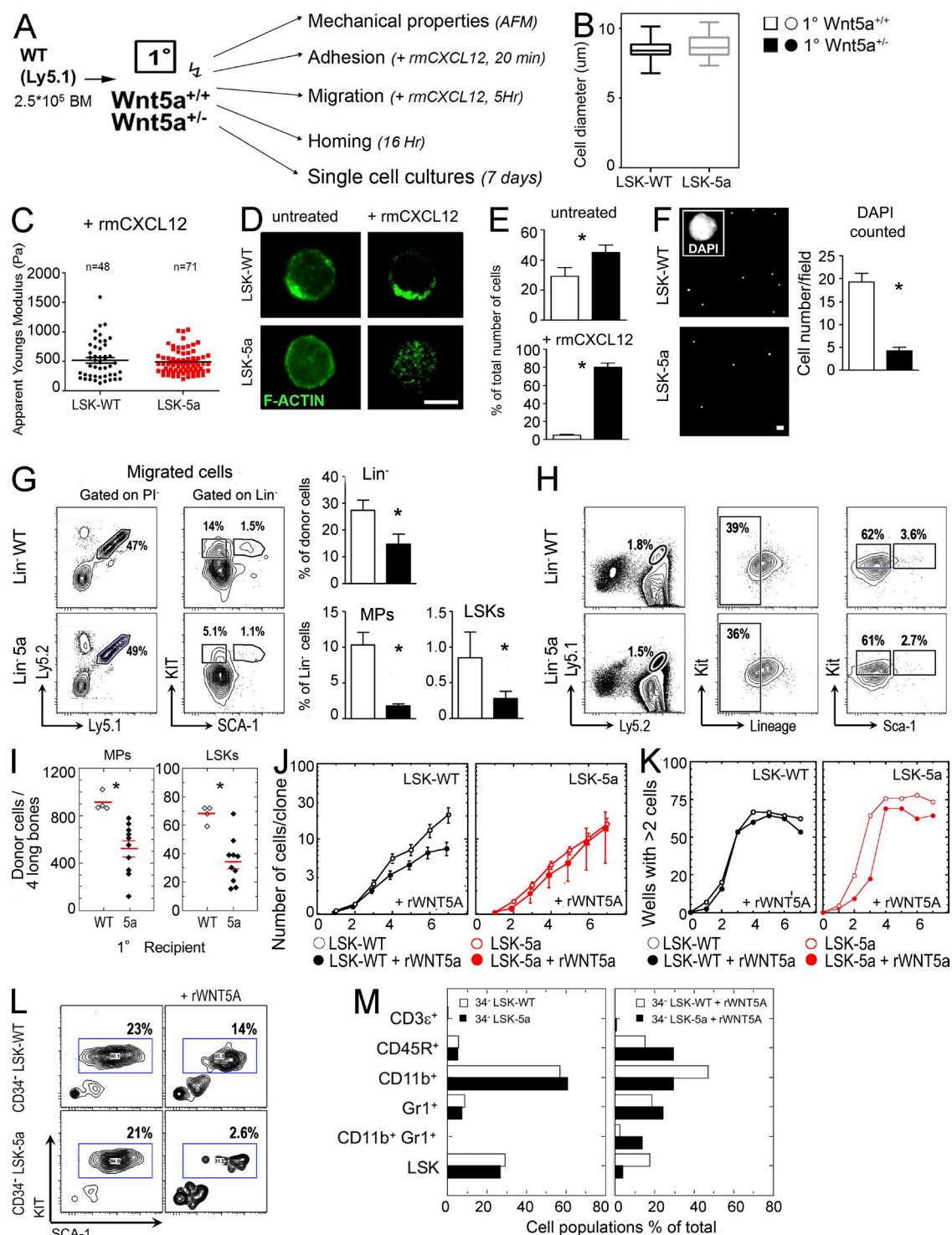
Figure 5. *Wnt5a*–deficient niche modulates actin-dependent cellular responses. (A) Experimental workflow. 16 wk after primary transplantation, LSKs were sorted from the BM of the 1° recipients of both genotypes and analyzed for mechanical cell properties, adhesion, migration, homing, and single cell cultures. (B) Cell diameters of 1° LSKs determined from phase-contrast images and presented as boxplots with 25th, 50th, and 75th percentiles denoted as horizontal lines, and 10th and 90th percentiles shown as whiskers. (C) The 1° LSKs adhering to a VCAM-1–coated surface were probed using an AFM cantilever equipped with 2.5-μm-radius bead. Experiments were conducted in the presence of 150 ng/ml rmCXCL12. Apparent Young's Moduli for individual cells (averaged for repeated measurements) are presented as dot plots. The number of probed cells is indicated. Mean apparent Young's Moduli of the probed cell population are denoted by horizontal lines. (D) The F-actin distribution in 1° LSK treated with 150 ng/ml rmCXCL12. (E) The percentages of cells with

and how these cells regenerate tissues. This process requires for the stem cells to find their anatomical niche, lodge there, and start regeneration of all cell types of the tissue. In transplantation settings, single HSCs efficiently lodge in the BM, and can repopulate the entire blood cell system. Our data show that the microenvironment significantly regulates the quality of the HSCs that are regenerated. We demonstrate that although HSCs efficiently engraft *Wnt5a*-haploinsufficient recipients, they are conditioned to show alterations in their transcriptome. In particular, we show dysregulated expression of several genes involved in the small GTPase-dependent actin polymerization pathway. These changes in gene expression result in reduced ability to form polarized F-actin bundles, leading to defects in adhesion, migratory behavior, and homing to the BM. Our results further suggest that the dysregulated gene expression in the *Wnt5a*-haploinsufficient environment is caused at least in part by up-regulated expression of targets of the transcription factor ZEB1.

Our study shows that the noncanonical Wnt5a not only signals through small GTPases but also regulates the amplitude of their response by up-regulating the expression of mediators of the small GTPase-dependent actin-regulatory pathway. Our results support the view that in LSK-5a this pathway is overactive, as we observed that F-actin polarization is defective as a result of CDC42 activation (Florian et al., 2012). Our results further show that this activation cannot be overcome by CXCL12 stimulation, which normally increases F-actin polarization (Voermans et al., 2001). The experiments reported here underscore the importance of the small GTPase pathway for different subprocesses of HSC engraftment: adhesion, migration, and homing. It has previously been shown that RAC1 (Cancelas et al., 2005) and CDC42 (Yang et al., 2007a) regulate HSC engraftment through acting on cell shape, localization and retention, and mobilization. Not only are the small GTPases themselves important, but upstream factors like DOCK2 (Kikuchi et al., 2008), ARHGAP5 (p190-B; Xu et al., 2009), ARHGEF7 (β-PIX; Reddy et al., 2016), or PTPRS (Quarmyne et al., 2015), or downstream factors such as PAK2 (Dorrance et al., 2013) and WASF2 (WAVE2; Ogaeri et al., 2009) also affect engraftment. Our study confirms these studies and adds that the niche regulates the generation of functional HSCs by modulating the activity of this pathway in HSCs not only through secretion of ligands such as the chemokine CXCL12 but also through modifications in the ex-

pression level of critical mediators of the pathway, such as β-PIX, DOCK2, and WAVE2.

We further show that the effects of altered gene expression of regenerated cells in a *Wnt5a*-haploinsufficient environment also affect *BCR–ABL*[p185+] cells, which, in 42% of the studied mice, fail to generate leukemia, and, in the remaining cases, fail to transfer leukemia to secondary mice. Similarly to the normal cells, *BCR–ABL*[p185+] cells from *Wnt5a*-haploinsufficient recipients show defects in the actin-regulation pathway and F-actin polarization, resulting in defective migration and secondary engraftment. The GTPase-dependent actin regulatory pathway has been described mostly to affect *BCR–ABL*[p210]-driven leukemogenesis, which, in contrast to *BCR–ABL*[p185], comprises the Bcr guanine exchange domain (Tala et al., 2013). It has been shown that RAC1 deficiency depletes *BCR–ABL*[p210] progenitors (Sengupta et al., 2010), and that the RAC1 and CDC42 exchange factor VAV drives leukemogenic proliferation and survival (Chang et al., 2012), as well as motility (Daubon et al., 2008). These studies and our findings suggest that coupling of small GTPase signals to actin polarization, which is required for directed migration may be a target to reduce leukemogenesis or to prevent reengraftment of leukemia after therapy, not only as has been suggested for *BCR–ABL*[p210] (Thomas et al., 2007) but also for *BCR–ABL*[p185].

Our study expands on current concepts of how the niche regulates the engraftment potential of HSCs, by showing that several different signaling mechanisms are simultaneously regulated. We and others have previously shown that secreted niche factors regulate engraftment through their effect on HSC cell cycle progression and self-renewal (Schreck et al., 2014). We here add to the concepts of niche regulation and demonstrate that the niche has a major extrinsic impact on the gene expression during the regeneration of the HSCs pool. In particular, reduced microenvironmental WNT5A causes defects in actin polymerization and cellular processes dependent on this signaling pathway. These findings with HSCs regenerated in a *Wnt5a*-haploinsufficient are reminiscent of aged HSCs, in particular with regard to reduction of short-term homing and LT-HSC frequency (Dykstra et al., 2011), as well as depolarization of F-actin localization and CDC42 activation (Florian et al., 2013). Our results, which reduced ability of HSCs to produce WNT5A does not rescue their failure to engraft secondary recipients, strongly suggest that although regeneration of hematopoiesis in a *Wnt5a*-hap-

---

apolar distribution of F-actin. Presented are the combined results of two independent experiments. (F) The pictures of adhered 1° LSKs on VCAM-1–coated slides stained with DAPI and counted. Presented are the results of three independent experiments. (G) FACS plots of 1° donor-type Lin⁻ cells (dot plots, left) migrated toward 150 ng/ml rmCXCL12 in the lower compartment of a Boyden camber (column graphs). These are the results of two independent experiments. (H) FACS plots of homed 1° LSKs cells in the BM 2° *WT* mice. (I) The total number of homed 1° LSKs the BM of 2° WT recipients. (J) The mean clone size of CD34⁻ LSK-WT and 5a cells cultured as single cells in conditioned medium from the UG26-1B6 cell line, supplemented with SCF and IL-11, with or without 500 ng/ml rWNT5A, counted each day for 7 d under the light microscope. (K) The total number of wells with more than two cells, shown over time. (L) FACS plots of Lin⁻ cells from pooled clones after 7 d culturing (Fig. S2). (M) The quantified percentage of lymphoid, myeloid, and LSK fractions of live cells. *, P < 0.05 (E, F, and G, Student's *t* test; I, MWU test).
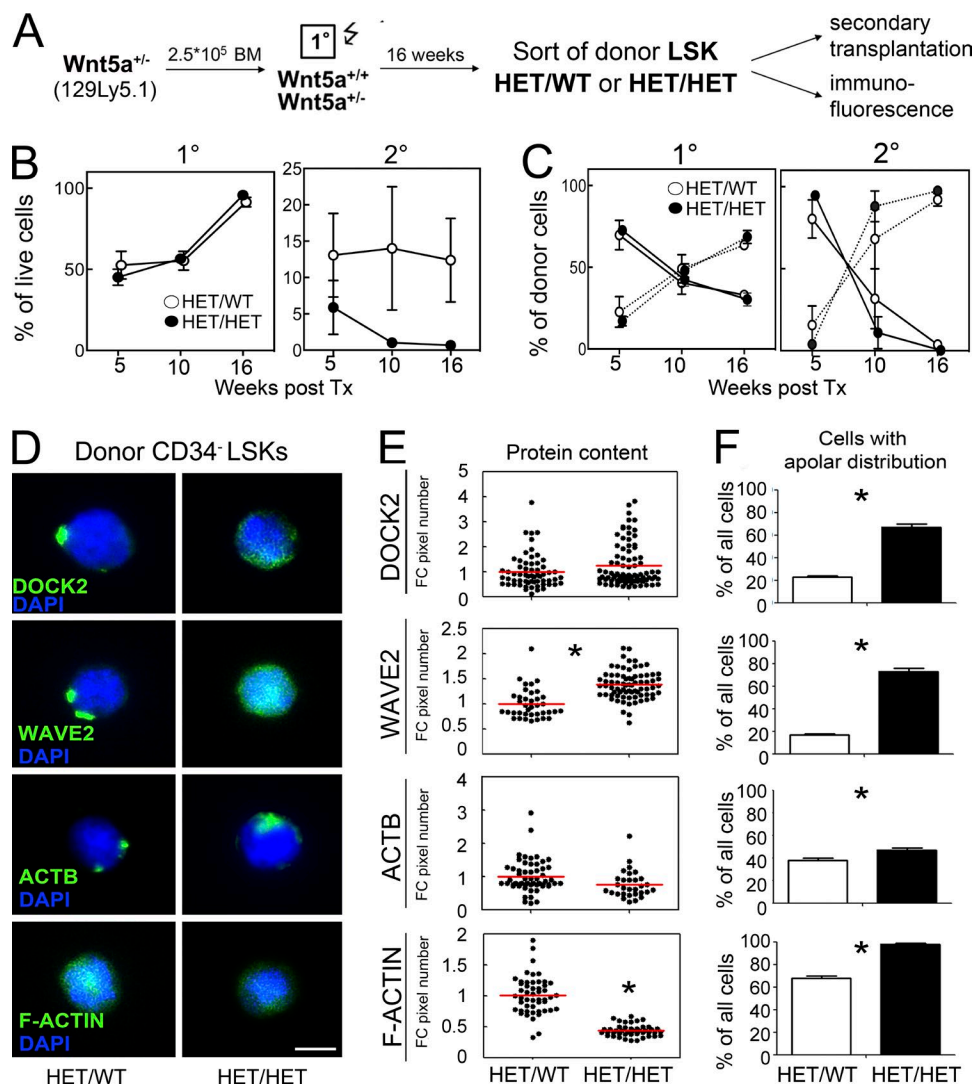
Figure 6. **Transplantation of donor *Wnt5a^(+/−)* HSCs in *WT* and *Wnt5a^(+/−)* recipient mice.** (A) Experimental design. Donor BM cells from *Wnt5a^(+/−)* were transplanted into *WT* or *Wnt5a^(+/−)* recipient mice. LSK cells were sorted from primary recipients and transplanted further into 2° *WT* animals. (B) The engraftment of 1° and 2° recipients. (C) Lymphoid (dotted line) and myeloid engraftment (solid line) for *Wnt5a^(+/−)* into WT (HET/WT, 1°, n = 15; 2°, n = 6) and *Wnt5a^(+/−)* into *Wnt5a^(+/−)* (HET/HET,1°, n = 6; 2°, n = 4). (D) Expression of DOCK2, WAVE2, ACTB, and F-actin in 1°CD34⁻ LSKs recovered from both genotype recipients. (E) The total pixel number of immunofluorescent staining quantified from 1° CD34⁻ LSKs with ImageJ software. (F) Assessment of polarized expression of the indicated proteins using ImageJ. *, P < 0.05 (MWU test).

loinsufficient environment shows similarities with aged mice, in regeneration, the niche appears to play a dominant role. Indeed, in previous studies comparing transcriptomes of young and old mice, the actin-regulatory pathway was only a minor dysregulated pathway (Sun et al., 2014), thus revealing the clear differences in regenerative and aging processes. A common denominator in both is CDC42 activation. However, the mechanisms through which this small GTPase is activated may differ and defining the different small GTPase activation pathways may offer new ways to improve tissue regeneration.

Our results show that reduction of WNT5A from the niche conditions HSCs during regeneration that this is not affected by cross-talk of HSCs which may up-regulate *Wnt5a*, as *Wnt5a*-haploinsufficient HSCs behave similar to WT HSCs. Interestingly though, in culture, the conditioned LT-LSK-5a are not rescued by addition of WNT5A. Instead, these cells almost completely differentiate into mature cell types, rapidly depleting LSK cells. Because WNT5A receptors and downstream mediators show no alterations in their expression, we hypothesize that the observed differentiation may be linked to actin regulation. Indeed, CDC42 is required for B cell differentiation (Guo et al., 2009) and regulates the balance between myelo- and erythropoiesis (Yang et al., 2007b). The related RAC1 GTPase is crucial for T-lympho-
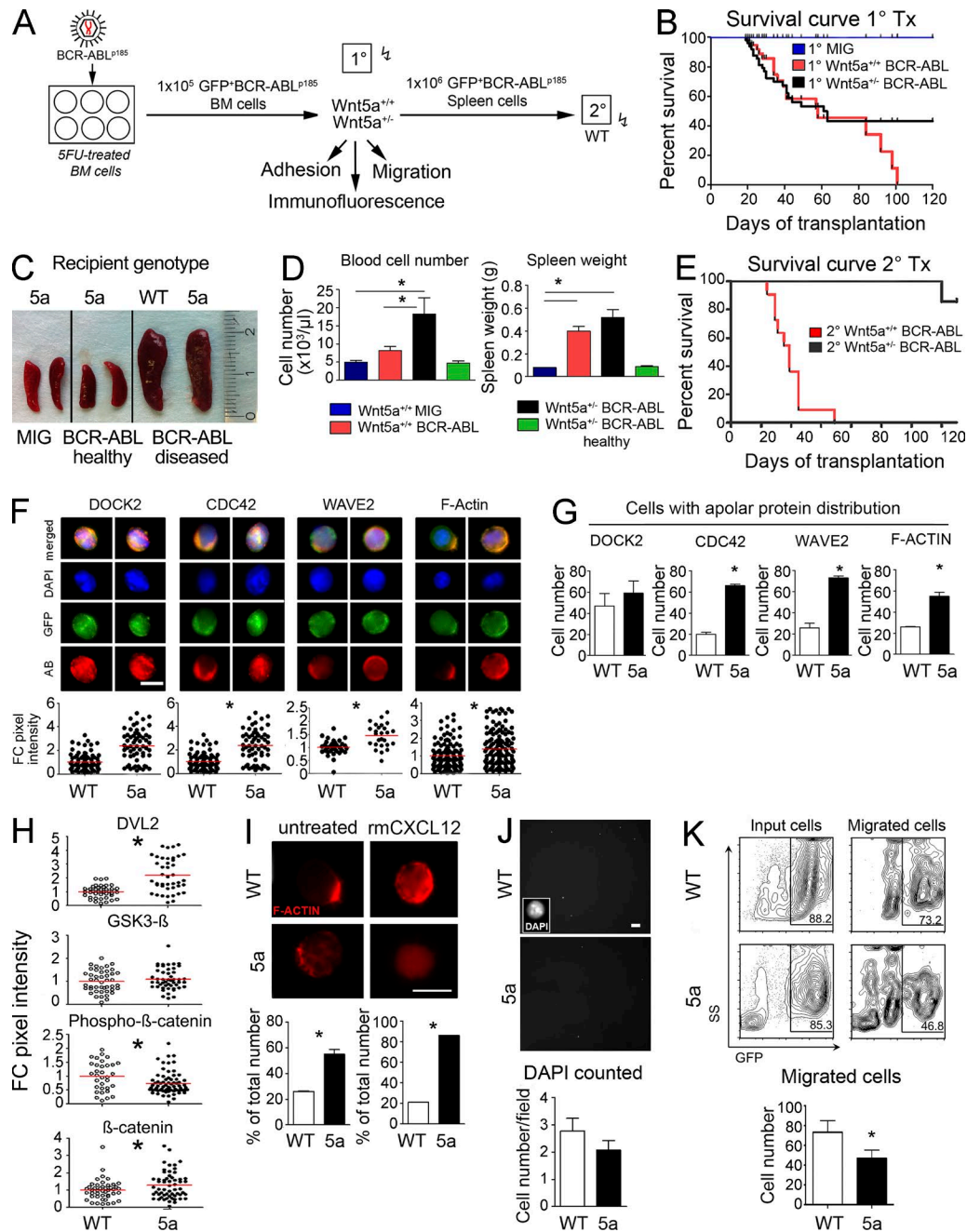
Figure 7. **Reduced *Wnt5a* in the niche affects development of BCR–ABL^p185 expressing cells.** (A) Experimental design. The BCR-ABL^p185 fusion protein was stably inserted via retroviral infection into the genome of BM cells from mice pretreated with 5FU. Further, 10^5 of GFP^+ cells were transplanted into 1° recipients of both genotypes. The mice were sacrificed when disease was apparent. All healthy recipient mice were sacrificed 120 d after Tx. 10^6 of 1° GFP^+ spleen cells were transplanted into 2° WT recipients. (B) Survival curve of 1° recipients (WT, *n* = 12; *Wnt5a*^+/−, *n* = 28). (C) Representative pictures of spleens from 1°recipients. (D) The blood cell number and the spleens size of 1° recipient mice. (E) Survival curve of 2° recipients (these are the results of three independent experiments; 2° from both WT and *Wnt5a*^+/− recipients, *n* = 11). (F) Expression of DOCK2, CDC42, WAVE2, and F-actin protein in 1° GFP^+ B220^+ B cells, counterstained with DAPI. The graphs represent fold change of the corresponding protein expression. (G) The numbers of cells with apolar protein distribution in 1° GFP^+ B220^+ cells. (H) The relative immunofluorescent staining for DVL, GSK3β, phospho-β-catenin, and β-catenin in 1° GFP^+B220^+ cells. (I) Representative pictures of F-actin distribution in 1° GFP^+ B220^+ of both genotypes treated or not with 150 ng/ml rmCXCL12. (J) The 1° GFP^+ B220^+ VCAM adhered to VCAM-coated slides and stained with DAPI. The graph displays the total cell nuclei counted per field, at least 10 fields were counted. (K) Representative FACS plots of migrated 1° GFP^+ B220^+ spleen cells toward 150 ng/ml rmCXCL12 in the lower chamber of a Boyden chamber. The graphs show absolute number of migrated 1° GFP^+ cells. Shown are the mean results of three independent experiments. *, P < 0.05 (D, G, I, and K, Student's *t* test; F and H, MWU test).

poiesis (Guo et al., 2008). Also, in Wiskott-Aldrich syndrome (WAS), a recessive disorder of WAS-family proteins, such as WAVE2, terminal differentiation of multiple blood cell lineages is reduced (Kajiwara et al., 1999). These findings suggest that study of the actin-regulatory pathway may lead to targets that can alter terminal differentiation outcomes.

Dysregulated actin polarization is not restricted to normal HSCs but also affects mature B cells and BCR–ABL[p185+] leukemic cells. Indeed, despite the fact that BCR–ABL is a strong oncogene, leukemic cells generated in the *Wnt5a*-haploinsufficient environment do not transfer leukemia, indicating that the actin-regulatory pathway is a possible therapeutic target to prevent reengraftment of hosts after initial therapy. We further present evidence suggesting that alterations in HSC gene expression by environmental Wnt5a may be caused by increased use of sequence motifs bound by the transcription factor ZEB1. In summary, our results reveal a novel mechanism by which the niche preserves HSC behavior required for successful engraftment. Extrinsic conditioning of gene expression patterns aids HSCs in their ability to adhere, migrate, and find their niches in times of stress. Our results further suggest that modulation of up- or downstream members of the actin-regulatory pathway could improve the regeneration of a functional stem cell pool.

MATERIALS AND METHODS
Mice
129S2 mice were obtained from Charles River and C57BL/6.J (B6, CD45.2) and B6.SJL-Ptprca.Pep3b/BoyJ (CD45.1) were obtained from Taconic. *Wnt5a*$^{+/-}$ (Yamaguchi et al., 1999) mice obtained from The Jackson Laboratory were backcrossed to the (129S2 x C57BL/6.J)F1 (129B6, CD45.2) background for at least six generations. Age- and gender-matched *Wnt5a*$^{+/+}$ (WT) littermates were used as controls in all experiments. In transplantation experiments, first-generation crosses of 129S2 and B6.SJL-Ptprca Pepcb/BoyJ (129Ly5.1, CD45.1xCD45.2) were used as recipients in intrinsic transplantation assays and as donors in extrinsic transplantations. All animal experiments were approved by the section Consumer Protection, Veterinary Services, and Food Hygiene of the Government of Upper Bavaria (Regierung Oberbayern, Munich, Germany). All animals were housed for at least a week before experimental use in microisolators under specific pathogen–free conditions, according to the Federation of Laboratory Animal Science Associations and institutional recommendations.

Flow cytometry analysis and cell sorting
Lin$^-$ SCA-1$^+$ Kit$^+$ (LSK) cells and further CD34$^-$ and CD150$^+$ subpopulations were isolated as described previously (Renström et al., 2009; Istvanffy et al., 2011). Surface antigens were stained with antibodies from eBioscience (Natutec), except for PE-Cy5.5-streptavidin conjugate, which was obtained from Invitrogen (Tables S1 and S2). FACS analyses were performed on a CyAn ADP Lx P8 (Coulter-Cytoma-

tion). Data were analyzed with FlowJo software (Tree Star). Sorting of cell populations was done with a MoFlo High Speed cell sorter (Beckman Coulter).

WNT5A intracellular FACS analysis
The intracellular staining was performed on endosteal cell fraction isolated from the four long bones, as previously described (Ruf et al., 2016). Antibodies used are listed in the Table S1. Stained cells were analyzed on CyAn ADPLx P8 (Beckman Coulter) flow cytometer.

Bone sections
8-μm bone sections of frozen femurs were prepared using the Kawamoto tape method (Kawamoto, 2003). In brief, bones were excised from mice, fixed, decalcified, and placed in sucrose before embedding in OCT and freezing. 8-μm sections of frozen femurs were then cut using the Leica tape system, stained with indicated antibodies overnight at 4°C, and images were acquired using an LSM710 microscope. Images were prepared using ImageJ (National Institutes of Health) software.

RNA sequencing (RNA-Seq)
RNA-sequencing data from donor-derived LSK cells was generated using the Smart-seq2 protocol and niche cell data were generated using UMI-seq, as described previously (Parekh et al., 2016). To remove noise from lowly expressed genes, count datasets were subjected to data-driven gene filtering using the HTSFilter R package (Rau et al., 2013; Tables S3 and S5).

Transcriptome analysis
Differential expression (DE) analysis was done by applying the DESeq2 package (Love et al., 2014) using the likelihood ratio to test for differential expression in 14,029 genes that fulfilled the test assumptions. Using an FDR <5% (Benjamini, 1995) as cut-off, 656 genes are differently expressed (Table S5). Overrepresentation of significantly DEGs in KEGG pathways (Table S6) was tested by a fixed network enrichment analysis implemented in the neaGUI R package (Alexeyenko et al., 2012). We used the topGO package (Alexa et al., 2006) for Gene Ontology (GO) enrichment analysis. Variance stabilized counts of all DEGs were plotted as heat map normalized to the mean value of LSK-WT cells. ISM ARA analysis (Balwierz et al., 2014) was done using default parameters, but without miRNA motifs because miRNAs had not been measured in our samples. Enrichment analysis (Fig. S3 G) was done using a Fisher's exact test categorizing the ISMARA annotated promoters by whether they are part of the actin regulation KEGG pathway and whether they are regulated by the tested motif.

Western blotting and CDC42–GTPase effector domain pull-down
For Wnt5a expression analysis, Western blotting was performed with lysates from BM primary stroma of *Wnt5a*$^{+/+}$

and *Wnt5a*^{+/−} mice containing 10% glycerol, 25 mM sodium fluoride, 1 mM sodium orthovanadate, and a protease inhibitor cocktail (Roche). After blotting the proteins on polyvinylidene difluoride membranes (EMD Millipore), 2% BSA in TBS with 0.1% Tween-20 was used for blocking and dilution of anti-Wnt5a antibody. Primary antibody was detected with an anti–rabbit horseradish peroxidase-conjugated secondary antibody and developed with the use of Super Signal chemiluminescent substrates.

Relative levels of GTP-bound CDC42 were determined by an effector pull-down assay. In brief, lineage-depleted BM cells (10^6) were lysed in a Mg^{2+} lysis/wash buffer (EMD Millipore), including protease inhibitors as in the previous paragraph. Samples were incubated with PAK-1–binding domain/agarose beads (EMD Millipore), and bound (activated) and unbound (nonactivated) CDC42 fractions were probed by immunoblotting with an anti-CDC42 antibody (rabbit polyclonal; EMD Millipore). Activated protein was normalized to total protein (Stain Free System; Bio-Rad Laboratories) and the relative amount was quantified by densitometry (ChemiDoc Imaging System; Bio-Rad Laboratories).

Single–cell immunofluorescence staining
As described previously (Renström et al., 2009; Istvanffy et al., 2011; Istvánffy et al., 2015), 500–1 × 10^3 sorted LSK-WT and LSK-5a cells or donor GFP^{+} B-cells were spotted on poly-ʟ-lysine-coated slides. In some experiments, 400–1,000 CD34^{+} or CD34^{−} LSK from different transplantation experiments were used. Cells were fixed with 4% paraformaldehyde in PBS, blocked with 10% FCS/0.1% Triton-X in PBS, and stained with primary and secondary antibodies listed in Tables S1 and S2. All stains were counterstained with SlowFade Gold Antifade Reagent with DAPI (Invitrogen). Staining was assessed using on a DM RBE fluorescent microscope (Leica). Fluorescence intensities of stained cells were quantified in total pixels using ImageJ. Each stain included a negative Ig control, the detected pixels of which were deducted from the total pictures as background.

Short–term colony assay
The number of colony-forming cells was determined with culture in growth factor–supplemented methylcellulose medium as described by the manufacturer (MethoCult GF M3434; StemCell Technologies).

Mechanical properties of LSK cells measured by atomic force microscopy (AFM) indentation
LSK cells adhering to a rhVCAM-coated surface were probed using an AFM cantilever equipped with a 2.5-μm-radius bead. Experiments were conducted in absence ("unstimulated") or presence ("+rmCXCL12") of 150 ng/ml murine rCXCL12 (R&D Systems). Apparent Young's Moduli for individual cells (from fits to the Hertz model, averaged for repeated measurements) are presented as dot plots. The number of probed cells is indicated. Mean apparent Young's Moduli of the probed cell

population are denoted by horizontal lines. Cell diameters were determined from phase contrast images and presented as boxplots with 25th, 50th, and 75th percentiles denoted as horizontal lines, and 10th and 90th percentiles as whiskers.

Adhesion assay
For adhesion assays, WT donor LSK cells regenerated in WT and *Wnt5a*^{+/−} primary recipients were sorted out after 16 wk, and 500 cells were spotted on slides coated with recombinant VCAM1 (R&D Systems) in PBS. The cells were stimulated 15 min after depositing with murine rCXCL12 (150 ng/ml: R&D Systems) and imaged on a DM RBE fluorescent microscope (Leica). Adhesion was calculated by measurement of light incidence with ImageJ.

Migration assays
A total of 600 μl IMDM supplemented with 2% FCS containing 150 ng/ml murine rCXCL12 was added to the lower chamber of a 24-well 5 μm transwell filter (Corning). Sorted Lin^{+} cells ($2 × 10^5$) in 100 μl IMDM were loaded to the upper chamber and were allowed to migrate for 4 h at 37°C. Migrating cells were collected from the lower chamber, stained for mature hematopoietic markers CD4, CD8a, CD11b, B220, and Gr-1, and counted using a CyAn ADP Lx P8 flow cytometer.

Homing assay
For this assay, 1,000 donor LSKs together with 30,000 donor MP cells sorted from the BM of WT and *Wnt5a*^{+/−} recipients, 16 wk after primary transplantation, were injected i.v. into secondary WT (C57BL/6.J) recipients. 16 h after i.v. injection, the secondary recipient mice were sacrificed and the BM were harvested. The homing ability of the WT cells was measured by quantifying the content of CD45.1^{+} donor cells by flow cytometry.

In vivo transplantation assay
Competitive repopulation was performed using transplantation of donor cells into lethally irradiated recipient mice, as described previously (Istvanffy et al., 2011; Istvánffy et al., 2015). For secondary and tertiary transplants, 129Ly5.1 (CD45.1xCD45.2)[+] Lin^{−} SCA-1^{+} KIT^{+} CD34^{−} CD150^{+} donor BM cells regenerated in primary recipients were used as donor cells, which were injected into lethally irradiated 129B6 (CD45.2) WT mice with freshly isolated 129B6 competitor cells (BM, 100,000; Spleen, 500,000).

Statistics
Unless otherwise indicated, the functional biological and the biochemical data are presented as the mean the standard error associated with the mean. In these experiments, the two-tailed Student's *t* test or the Mann-Whitney *U* test for independent samples (MWU test) with a level of significance set at 0.05 were performed for two-group comparisons of the differences between the samples under study. In the analyses

of the RNA-seq data, we used the FDR to control for the expected proportion of false discoveries among the rejected hypotheses (Benjamini, 1995).

Data accession

Sequence reads from the RNA sequencing can be accessed at the Gene Expression Omnibus under accession no. GSE84993.

Online supplemental material

Fig. S1 shows gating of BM staining of primary, secondary, and tertiary transplantations (related to Fig. 1). Fig. S2 show gating of single-cell culture of donor CD34⁻ LSK cells isolated from transplanted WT and $Wnt5a^{+/-}$ recipients (related to Fig. 5). Fig. S3 shows flow cytometry of primary BCR–ABL^{p185}–leukemic mice (related to Fig. 7). Tables S1–S6 are available as Excel files. Table S1 lists primary antibodies used in this study. Table S2 lists secondary reagents and antibodies used in this study. Table S3 is a comparison of mapped RNA sequences from MSC-WT and MSC-5a. Table S4 lists GO enrichment analysis of MSC transcriptomes from transplanted recipients. Table S5 is a comparison of mapped RNA sequences from LSK-WT and LSK-5a. Table S6 lists KEGG pathway enrichment analysis of the genes differentially expressed between LSK-WT and LSK-5a.

REFERENCES

Abrahamsson, A.E., I. Geron, J. Gotlib, K.H. Dao, C.F. Barroga, I.G. Newton, F.J. Giles, J. Durocher, M. Karimi, et al. 2009. Glycogen synthase kinase 3beta missplicing contributes to leukemia stem cell generation. *Proc. Natl. Acad. Sci. USA.* 106:3925–3929. http://dx.doi.org/10.1073/pnas.0900189106

Alexa, A., J. Rahnenführer, and T. Lengauer. 2006. Improved scoring of functional groups from gene expression data by decorrelating GO graph structure. *Bioinformatics.* 22:1600–1607. http://dx.doi.org/10.1093/bioinformatics/btl140

Alexeyenko, A., W. Lee, M. Pernemalm, J. Guegan, P. Dessen, V. Lazar, J. Lehtiö, and Y. Pawitan. 2012. Network enrichment analysis: extension of gene-set enrichment analysis to gene networks. *BMC Bioinformatics.* 13:226. http://dx.doi.org/10.1186/1471-2105-13-226

Balwierz, P.J., M. Pachkov, P. Arnold, A.J. Gruber, M. Zavolan, and E. van Nimwegen. 2014. ISMARA: automated modeling of genomic signals as a democracy of regulatory motifs. *Genome Res.* 24:869–884. http://dx.doi.org/10.1101/gr.169508.113

Benjamini, Y.H.Y. 1995. Controlling the false discovery rate: a powerful and practical approach to multiple testing. *J. R. Stat. Soc. B.* 57:289–300.

Buckley, S.M., F. Ulloa-Montoya, D. Abts, R.A. Oostendorp, E. Dzierzak, S.C. Ekker, and C.M. Verfaillie. 2011. Maintenance of HSC by Wnt5a secreting AGM-derived stromal cell line. *Exp. Hematol.* 39:114–123.e1: 5. http://dx.doi.org/10.1016/j.exphem.2010.09.010

Cancelas, J.A., A.W. Lee, R. Prabhakar, K.F. Stringer, Y. Zheng, and D.A. Williams. 2005. Rac GTPases differentially integrate signals regulating hematopoietic stem cell localization. *Nat. Med.* 11:886–891. http://dx.doi.org/10.1038/nm1274

Chang, K.H., A. Sanchez-Aguilera, S. Shen, A. Sengupta, M.N. Madhu, A.M. Ficker, S.K. Dunn, A.M. Kuenzi, J.L. Arnett, R.A. Santho, et al. 2012. Vav3 collaborates with p190-BCR-ABL in lymphoid progenitor leukemogenesis, proliferation, and survival. *Blood.* 120:800–811. http://dx.doi.org/10.1182/blood-2011-06-361709

Daubon, T., J. Chasseriau, A. El Ali, J. Rivet, A. Kitzis, B. Constantin, and N. Bourmeyster. 2008. Differential motility of p190bcr-abl- and p210bcr-abl-expressing cells: respective roles of Vav and Bcr-Abl GEFs. *Oncogene.* 27:2673–2685. http://dx.doi.org/10.1038/sj.onc.1210933

Dijksterhuis, J.P., J. Petersen, and G. Schulte. 2014. WNT/Frizzled signalling: receptor-ligand selectivity with focus on FZD-G protein signalling and its physiological relevance: IUPHAR Review 3. *Br. J. Pharmacol.* 171:1195–1209. http://dx.doi.org/10.1111/bph.12364

Dorrance, A.M., S. De Vita, M. Radu, P.N. Reddy, M.K. McGuinness, C.E. Harris, R. Mathieu, S.W. Lane, R. Kosoff, M.D. Milsom, et al. 2013. The Rac GTPase effector p21-activated kinase is essential for hematopoietic stem/progenitor cell migration and engraftment. *Blood.* 121:2474–2482. http://dx.doi.org/10.1182/blood-2012-10-460709

Dykstra, B., S. Olthof, J. Schreuder, M. Ritsema, and G. de Haan. 2011. Clonal analysis reveals multiple functional defects of aged murine hematopoietic stem cells. *J. Exp. Med.* 208:2691–2703. http://dx.doi.org/10.1084/jem.20111490

Florian, M.C., K. Dörr, A. Niebel, D. Daria, H. Schrezenmeier, M. Rojewski, M.D. Filippi, A. Hasenberg, M. Gunzer, K. Scharffetter-Kochanek, et al. 2012. Cdc42 activity regulates hematopoietic stem cell aging and rejuvenation. *Cell Stem Cell.* 10:520–530. http://dx.doi.org/10.1016/j.stem.2012.04.007

Florian, M.C., K.J. Nattamai, K. Dörr, G. Marka, B. Uberle, V. Vas, C. Eckl, I. Andrä, M. Schiemann, R.A. Oostendorp, et al. 2013. A canonical to non-canonical Wnt signalling switch in haematopoietic stem-cell ageing. *Nature.* 503:392–396. http://dx.doi.org/10.1038/nature12631

Guo, F., J.A. Cancelas, D. Hildeman, D.A. Williams, and Y. Zheng. 2008. Rac GTPase isoforms Rac1 and Rac2 play a redundant and crucial role in T-cell development. *Blood.* 112:1767–1775. http://dx.doi.org/10.1182/blood-2008-01-132068

Guo, F., C.S. Velu, H.L. Grimes, and Y. Zheng. 2009. Rho GTPase Cdc42 is essential for B-lymphocyte development and activation. *Blood.* 114:2909–2916. http://dx.doi.org/10.1182/blood-2009-04-214676

Istvanffy, R., M. Kröger, C. Eckl, S. Gitzelmann, B. Vilne, F. Bock, M. Schiemann, U.B. Keller, C. Peschel, and R.A. Oostendorp. 2011. Stromal pleiotrophin regulates repopulation behavior of hematopoietic stem cells. *Blood.* 118:2712–2722. http://dx.doi.org/10.1182/blood-2010-05-287235

Istvánffy, R., B. Vilne, C. Schreck, F. Ruf, C. Pagel, S. Grziwok, L. Henkel, O. Prazeres da Costa, J. Berndt, V. Stümpflen, et al. 2015. Stroma-derived connective tissue growth factor maintains cell cycle progression and

repopulation activity of hematopoietic stem cells in vitro. *Stem Cell Rep.* 5:702–715. http://dx.doi.org/10.1016/j.stemcr.2015.09.018

Kajiwara, M., S. Nonoyama, M. Eguchi, T. Morio, K. Imai, H. Okawa, M. Kaneko, M. Sako, S. Ohga, M. Maeda, et al. 1999. WASP is involved in proliferation and differentiation of human haemopoietic progenitors in vitro. *Br. J. Haematol.* 107:254–262. http://dx.doi.org/10.1046/j.1365 -2141.1999.01694.x

Kawamoto, T. 2003. Use of a new adhesive film for the preparation of multi- purpose fresh-frozen sections from hard tissues, whole-animals, insects and plants. *Arch. Histol. Cytol.* 66:123–143. http://dx.doi.org/10.1679 /aohc.66.123

Kelliher, M., A. Knott, J. McLaughlin, O.N. Witte, and N. Rosenberg. 1991. Differences in oncogenic potency but not target cell specificity distinguish the two forms of the BCR/ABL oncogene. *Mol. Cell. Biol.* 11:4710–4716. http://dx.doi.org/10.1128/MCB.11.9.4710

Khan, J.A., A. Mendelson, Y. Kunisaki, A. Birbrair, Y. Kou, A. Arnal-Estapé, S. Pinho, P. Ciero, F. Nakahara, A. Ma'ayan, et al. 2016. Fetal liver hematopoietic stem cell niches associate with portal vessels. *Science.* 351:176–180. http://dx.doi.org/10.1126/science.aad0084

Kikuchi, T., S. Kubonishi, M. Shibakura, N. Namba, T. Matsui, Y. Fukui, M. Tanimoto, and Y. Katayama. 2008. Dock2 participates in bone marrow lympho-hematopoiesis. *Biochem. Biophys. Res. Commun.* 367:90–96. http ://dx.doi.org/10.1016/j.bbrc.2007.12.093

Lento, W., T. Ito, C. Zhao, J.R. Harris, W. Huang, C. Jiang, K. Owzar, S. Piryani, L. Racioppi, N. Chao, and T. Reya. 2014. Loss of β-catenin triggers oxidative stress and impairs hematopoietic regeneration. *Genes Dev.* 28:995–1004. http://dx.doi.org/10.1101/gad.231944.113

Li, S., R.L. Ilaria Jr., R.P. Million, G.Q. Daley, and R.A. Van Etten. 1999. The P190, P210, and P230 forms of the BCR/ABL oncogene induce a similar chronic myeloid leukemia-like syndrome in mice but have different lymphoid leukemogenic activity. *J. Exp. Med.* 189:1399–1412. http://dx.doi.org/10.1084/jem.189.9.1399

Liang, H., Q. Chen, A.H. Coles, S.J. Anderson, G. Pihan, A. Bradley, R. Gerstein, R. Jurecic, and S.N. Jones. 2003. Wnt5a inhibits B cell proliferation and functions as a tumor suppressor in hematopoietic tissue. *Cancer Cell.* 4:349–360. http://dx.doi.org/10.1016/S1535-6108(03)00268-X

Love, M.I., W. Huber, and S. Anders. 2014. Moderated estimation of fold change and dispersion for RNA-seq data with DESeq2. *Genome Biol.* 15:550. http://dx.doi.org/10.1186/s13059-014-0550-8

Luis, T.C., B.A. Naber, P.P. Roozen, M.H. Brugman, E.F. de Haas, M. Ghazvini, W.E. Fibbe, J.J. van Dongen, R. Fodde, and F.J. Staal. 2011. Canonical wnt signaling regulates hematopoiesis in a dosage-dependent fashion. *Cell Stem Cell.* 9:345–356. http://dx.doi.org/10.1016/j.stem.2011.07.017

Murdoch, B., K. Chadwick, M. Martin, F. Shojaei, K.V. Shah, L. Gallacher, R.T. Moon, and M. Bhatia. 2003. Wnt-5A augments repopulating capacity and primitive hematopoietic development of human blood stem cells in vivo. *Proc. Natl. Acad. Sci. USA.* 100:3422–3427. http://dx .doi.org/10.1073/pnas.013023310012626754

Nemeth, M.J., L. Topol, S.M. Anderson, Y. Yang, and D.M. Bodine. 2007. Wnt5a inhibits canonical Wnt signaling in hematopoietic stem cells and enhances repopulation. *Proc. Natl. Acad. Sci. USA.* 104:15436–15441. http ://dx.doi.org/10.1073/pnas.0704747104

Ogaeri, T., K. Eto, M. Otsu, H. Ema, and H. Nakauchi. 2009. The actin polymerization regulator WAVE2 is required for early bone marrow repopulation by hematopoietic stem cells. *Stem Cells.* 27:1120–1129. http://dx.doi.org/10.1002/stem.42

Parekh, S., C. Ziegenhain, B. Vieth, W. Enard, and I. Hellmann. 2016. The impact of amplification on differential expression analyses by RNA-seq. *Sci. Rep.* 6:25533. http://dx.doi.org/10.1038/srep25533

Quarmyne, M., P.L. Doan, H.A. Himburg, X. Yan, M. Nakamura, L. Zhao, N.J. Chao, and J.P. Chute. 2015. Protein tyrosine phosphatase-σ regulates hematopoietic stem cell-repopulating capacity. *J. Clin. Invest.* 125:177– 182. http://dx.doi.org/10.1172/JCI77866

Rau, A., M. Gallopin, G. Celeux, and F. Jaffrézic. 2013. Data-based filtering for replicated high-throughput transcriptome sequencing experiments. *Bioinformatics.* 29:2146–2152. http://dx.doi.org/10.1093/bioinformatics /btt350

Rauner, M., N. Stein, M. Winzer, C. Goettsch, J. Zwerina, G. Schett, J.H. Distler, J. Albers, J. Schulze, T. Schinke, et al. 2012. WNT5A is induced by inflammatory mediators in bone marrow stromal cells and regulates cytokine and chemokine production. *J. Bone Miner. Res.* 27:575–585. http://dx.doi.org/10.1002/jbmr.1488

Reddy, P.N., M. Radu, K. Xu, J. Wood, C.E. Harris, J. Chernoff, and D.A. Williams. 2016. p21-activated kinase 2 regulates HSPC cytoskeleton, migration, and homing via CDC42 activation and interaction with β-Pix. *Blood.* 127:1967–1975. http://dx.doi.org/10.1182/blood-2016 -01-693572

Renström, J., R. Istvanffy, K. Gauthier, A. Shimono, J. Mages, A. Jardon- Alvarez, M. Kröger, M. Schiemann, D.H. Busch, I. Esposito, et al. 2009. Secreted frizzled-related protein 1 extrinsically regulates cycling activity and maintenance of hematopoietic stem cells. *Cell Stem Cell.* 5:157–167. http://dx.doi.org/10.1016/j.stem.2009.05.020

Ruf, F., C. Schreck, A. Wagner, C. Pagel, S. Romero, M. Kieslinger, A. Shimono, C. Peschel, K.S. Götze, et al. 2016. Loss of Sfrp2 in the niche amplifies stress-induced cellular responses, and impairs the in vivo regeneration of the hematopoietic stem cell pool. *Stem Cells.* 34:2381– 2392. http://dx.doi.org/10.1002/stem.2416

Schreck, C., F. Bock, S. Grziwok, R.A. Oostendorp, and R. Istvánffy. 2014. Regulation of hematopoiesis by activators and inhibitors of Wnt signaling from the niche. *Ann. N.Y. Acad. Sci.* 1310:32–43. http://dx.doi .org/10.1111/nyas.12384

Sengupta, A., J. Arnett, S. Dunn, D.A. Williams, and J.A. Cancelas. 2010. Rac2 GTPase deficiency depletes BCR-ABL+ leukemic stem cells and progenitors in vivo. *Blood.* 116:81–84. http://dx.doi.org/10.1182/blood -2009-10-247437

Sun, D., M. Luo, M. Jeong, B. Rodriguez, Z. Xia, R. Hannah, H. Wang, T. Le, K.F. Faull, R. Chen, et al. 2014. Epigenomic profiling of young and aged HSCs reveals concerted changes during aging that reinforce self- renewal. *Cell Stem Cell.* 14:673–688. http://dx.doi.org/10.1016/j.stem .2014.03.002

Tala, I., R. Chen, T. Hu, E.R. Fitzpatrick, D.A. Williams, and I.P. Whitehead. 2013. Contributions of the RhoGEF activity of p210 BCR/ABL to disease progression. *Leukemia.* 27:1080–1089. http://dx.doi.org/10 .1038/leu.2012.351

Thomas, E.K., J.A. Cancelas, H.D. Chae, A.D. Cox, P.J. Keller, D. Perrotti, P. Neviani, B.J. Druker, K.D. Setchell, Y. Zheng, et al. 2007. Rac guanosine triphosphatases represent integrating molecular therapeutic targets for BCR-ABL-induced myeloproliferative disease. *Cancer Cell.* 12:467–478. http://dx.doi.org/10.1016/j.ccr.2007.10.015

Voermans, C., E.C. Anthony, E. Mul, E. van der Schoot, and P. Hordijk. 2001. SDF-1-induced actin polymerization and migration in human hematopoietic progenitor cells. *Exp. Hematol.* 29:1456–1464. http://dx .doi.org/10.1016/S0301-472X(01)00740-8

Wang, Y., A.V. Krivtsov, A.U. Sinha, T.E. North, W. Goessling, Z. Feng, L.I. Zon, and S.A. Armstrong. 2010. The Wnt/beta-catenin pathway is required for the development of leukemia stem cells in AML. *Science.* 327:1650–1653. http://dx.doi.org/10.1126/science.1186624

Wohrer, S., D.J. Knapp, M.R. Copley, C. Benz, D.G. Kent, K. Rowe, S. Babovic, H. Mader, R.A. Oostendorp, and C.J. Eaves. 2014. Distinct stromal cell factor combinations can separately control hematopoietic stem cell survival, proliferation, and self-renewal. *Cell Reports.* 7:1956–1967. http ://dx.doi.org/10.1016/j.celrep.2014.05.014

Xu, H., S. Eleswarapu, H. Geiger, K. Szczur, D. Daria, Y. Zheng, J. Settleman, E.F. Srour, D.A. Williams, and M.D. Filippi. 2009. Loss of the Rho GTPase activating protein p190-B enhances hematopoietic stem cell

engraftment potential. *Blood*. 114:3557–3566. http://dx.doi.org/10 .1182/blood-2009-02-205815

Yamaguchi, T.P., A. Bradley, A.P. McMahon, and S. Jones. 1999. A Wnt5a pathway underlies outgrowth of multiple structures in the vertebrate embryo. *Development*. 126:1211–1223.

Yang, L., L. Wang, H. Geiger, J.A. Cancelas, J. Mo, and Y. Zheng. 2007a. Rho GTPase Cdc42 coordinates hematopoietic stem cell quiescence and niche interaction in the bone marrow. *Proc. Natl. Acad. Sci. USA*. 104:5091–5096. http://dx.doi.org/10.1073/pnas.0610819104

Yang, L., L. Wang, T.A. Kalfa, J.A. Cancelas, X. Shang, S. Pushkaran, J. Mo, D.A. Williams, and Y. Zheng. 2007b. Cdc42 critically regulates the balance between myelopoiesis and erythropoiesis. *Blood*. 110:3853–3861. http:// dx.doi.org/10.1182/blood-2007-03-079582

Zhao, C., J. Blum, A. Chen, H.Y. Kwon, S.H. Jung, J.M. Cook, A. Lagoo, and T. Reya. 2007. Loss of beta-catenin impairs the renewal of normal and CML stem cells in vivo. *Cancer Cell*. 12:528–541. http://dx.doi.org/10 .1016/j.ccr.2007.11.003

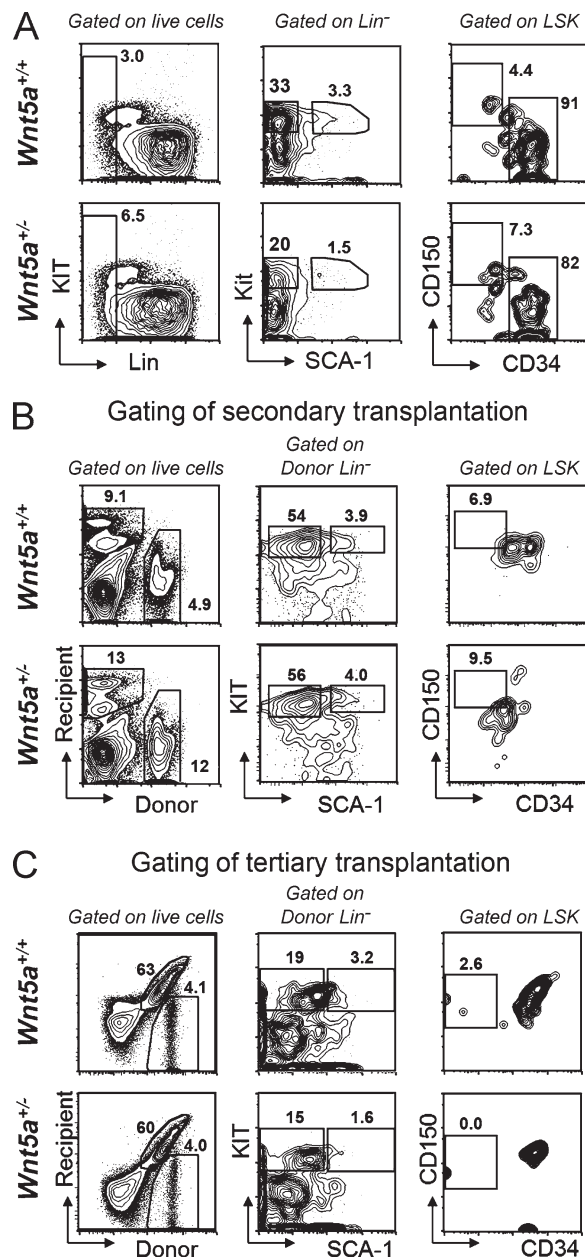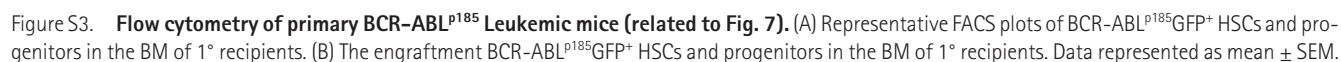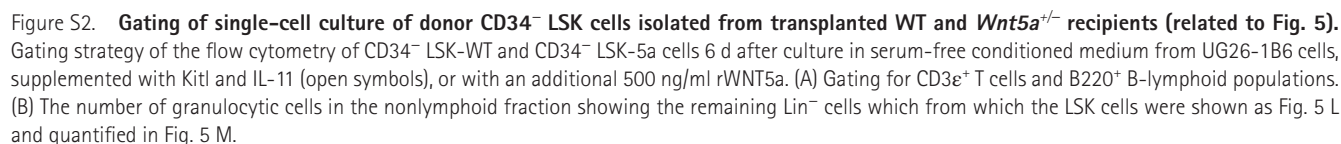Schreck et al., https://doi.org/10.1084/jem.20151414

Figure S1.   **Gating of BM staining of primary, secondary, and tertiary transplantations (related to Fig. 1).** (A) Representative FACS plots of BM from 1° recipients isolated 16 wk after transplantation. (B) Similar plots from 2° recipients (C) and also for the 3° transplantations.

Figure S2. **Gating of single–cell culture of donor CD34⁻ LSK cells isolated from transplanted WT and *Wnt5a*⁺/⁻ recipients (related to Fig. 5).** Gating strategy of the flow cytometry of CD34⁻ LSK-WT and CD34⁻ LSK-5a cells 6 d after culture in serum-free conditioned medium from UG26-1B6 cells, supplemented with Kitl and IL-11 (open symbols), or with an additional 500 ng/ml rWNT5a. (A) Gating for CD3ε⁺ T cells and B220⁺ B-lymphoid populations. (B) The number of granulocytic cells in the nonlymphoid fraction showing the remaining Lin⁻ cells which from which the LSK cells were shown as Fig. 5 L and quantified in Fig. 5 M.

Figure S3. **Flow cytometry of primary BCR–ABL^p185 Leukemic mice (related to Fig. 7).** (A) Representative FACS plots of BCR–ABL^p185GFP⁺ HSCs and progenitors in the BM of 1° recipients. (B) The engraftment BCR–ABL^p185GFP⁺ HSCs and progenitors in the BM of 1° recipients. Data represented as mean ± SEM.

Tables S1–S6 are available as Excel files. Table S1 lists primary antibodies used in this study. Table S2 lists secondary reagents and antibodies used in this study. Table S3 is a comparison of mapped RNA sequences from MSC–WT and MSC–5a. Table S4 lists GO enrichment analysis of MSC transcriptomes from transplanted recipients. Table S5 is a comparison of mapped RNA sequences from LSK–WT and LSK–5a. Table S6 lists KEGG pathway enrichment analysis of the genes differentially expressed between LSK–WT and LSK–5a.